SCIENCE CHINA
Earth Sciences

SPECIAL TOPIC: Microbeam Analytical Techniques and Their Applications to Earth Science
• RESEARCH PAPER •

October 2015 Vol.58 No.10: 1758–1767
doi: 10.1007/s11430-015-5106-6

NanoSIMS analytical technique and its applications in earth sciences

YANG Wei*, HU Sen, ZHANG JianChao, HAO JiaLong & LIN YangTing

Key Laboratory of Earth and Planetary Physics, Institute of Geology and Geophysics, Chinese Academy of Sciences, Beijing 100029, China

Received November 10, 2014; accepted March 30, 2015; published online June 4, 2015

Despite the significant improvement on spatial resolution, NanoSIMS still preserves relatively high mass resolution, sensitivity, and analytical precision. It has become an important analytical platform to determine chemical compositions of solid materials, and has been widely used in space, earth, life, and materials sciences, etc. By using a Cs^+ ion beam with a size as small as 50 nm scanning over sample surfaces, we are able to obtain high spatial resolution images of up to 7 species simultaneously. When utilizing Faraday cup, high analytical precision of 0.3‰–0.5‰ (1SD) for C, O and S isotopic analysis can be achieved. Although this precision level is still lower than that of conventional SIMS, it already meets the major requirements of Earth Sciences. In 2011, the first NanoSIMS of China (Cameca NanoSIMS 50L) was installed at Institute of Geology and Geophysics, Chinese Academy of Sciences. Based on the working mechanism and analytical modes of the instrument, this paper will systematically introduce the analytical methods established with the NanoSIMS and their potential applications in earth sciences. These methods include trace element distribution images in mineral zoning, high spatial resolution (2–5 μm) Pb-Pb and U-Pb dating, water content and H isotopic analysis for silicate glass and apatite, C isotopic analysis for diamond and graphite, O isotopic analysis for carbonate, S isotopic analysis for sulfides. In addition, the specific requirements for sample preparation will also be introduced in order to facilitate domestic earth scientists' use.

NanoSIMS, micro-beam analysis, elemental distribution images, Pb-Pb and U-Pb dating, stable isotopes

Citation: Yang W, Hu S, Zhang J C, Hao J L, Lin Y T. 2015. NanoSIMS analytical technique and its applications in earth sciences. Science China: Earth Sciences, 58: 1758−1767, doi: 10.1007/s11430-015-5106-6

Modern advances in micro-beam analytical technique, on one hand, significantly improve analytical precision, which is even comparable to those of methods with chemical separation and purification. On the other hand, spatial resolution has also been significantly improved by reducing the size of the micro-beam from micron scale to sub-micron or nanometer scale. For Secondary Ion Mass Spectrometry (SIMS), the latest type Cameca IMS-1280HR is characterized by its high analytical precision, whereas Cameca NanoSIMS 50L is by its high spatial resolution.

The initial demands on NanoSIMS came mainly from two aspects: one is from space sciences, searching micron and submicron size pre-solar grains in extraterrestrial samples, and analyzing their isotopic compositions (Hoppe, 2006; Messenger et al., 2003; Zinner et al., 2011); the other is from life sciences, tracing stable isotopic variations at subcellular scale (Herrmann et al., 2007; Lechene et al., 2006, 2007; Musat et al., 2008). Due to the ultra-high spatial resolution of NanoSIMS, its application quickly expanded to material sciences (Dark et al., 2006; McPhail, 2006) and earth Sciences (Badro et al., 2007; Meibom et al., 2008). Nowadays, due to the advances on secondary ion transmission efficiency and mass resolution, analytical precision of stable isotopes by NanoSIMS has also been significantly improved. For example, high precisions of

*Corresponding author (email: yangw@mail.iggcas.ac.cn)

0.3‰–0.5‰ (1SD) for C, O and S isotopes can be achieved, which largely broadens the application of NanoSIMS in the earth sciences.

Since the first commercial NanoSIMS installed in 2000, there are more than 30 NanoSIMSs in the world at present. The instrument has updated from Cameca NanoSIMS 50 (5 detectors) to NanoSIMS 50L (7 detectors). In 2011, the first NanoSIMS of China (Cameca NanoSIMS 50L) was installed at Institute of Geology and Geophysics, Chinese Academy of Sciences. After more than 3 years' development, a variety of analytical methods have been established with this instrument, providing a bran-new platform for basic researches on space, life, earth and materials sciences. Based on the working mechanism and analytical modes of the instrument, this paper will systematically introduce the analytical methods established with this instrument and their potential applications in earth sciences. In addition, the specific requirements for sample preparation will also be introduced in order to facilitate domestic earth scientists' use.

1 Mechanism and analytical modes of NanoSIMS

Secondary Ion Mass Spectrometry (SIMS) is a type of mass spectrometry, which can analyze *In situ* chemical compositions of solid materials. The working mechanism of SIMS is as follow: A primary ion beam generated from an ion source is accelerated to sputter the surface of a solid sample. The ion bombardment triggered by the primary ion beam can lead to emission of secondary ions from the sample surface. Then, the secondary ions are analyzed and collected by a mass spectrometry, and based on the count rates of secondary ions, the elemental abundances and isotopic compositions of the sample can be calculated (Figure 1). The detailed introductions of SIMS, such as its history, development, mechanism, and applications, have been previously reviewed (Hsu, 2005; Li et al., 2013a). At present, SIMS is able to analyze all the elements in the periodic table except noble gas. There are dozens of laboratories worldwide equipped with SIMS of SHRIMP series, Cameca IMS series, or Cameca NanoSIMS.

1.1 Working mechanism of NanoSIMS

As an *in situ* analytical instrument of chemical composition, the performance of SIMS lies in the following aspects: spatial resolution, sensitivity, mass resolution, and precision. The spatial resolution depends on the generation and focusing of the primary ion beam, which can reach 1 μm by conventional SIMS (Page et al., 2007). Sensitivity depends on yield of the secondary ions and transmission efficiency. Mass resolution depends mainly on the magnet performance. Precision, on one hand, depends on the stability of the whole instrument, and on the other hand, relies on the standards and analytical methods.

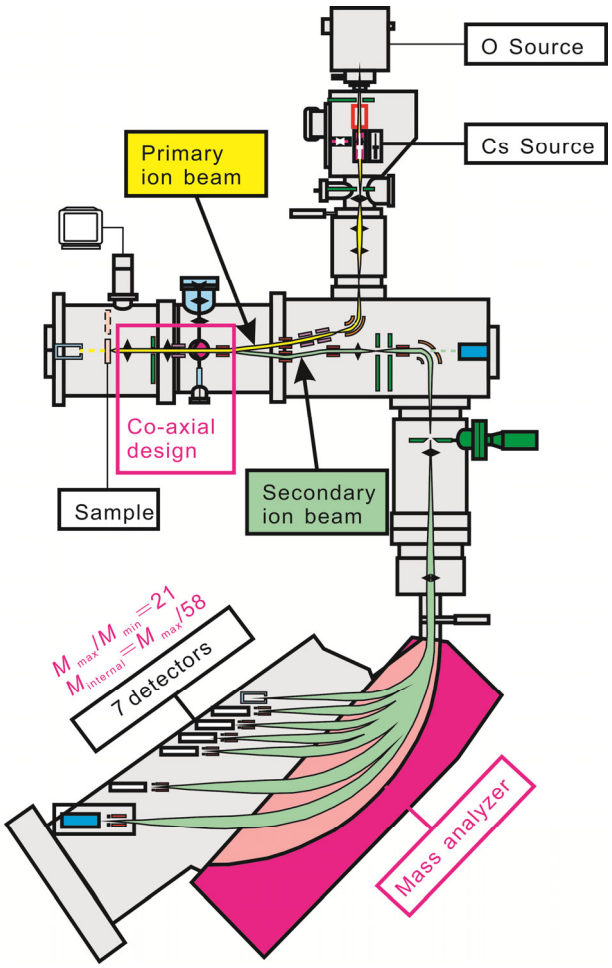

Figure 1 Schematic diagram showing structure of Cameca NanoSIMS 50L. The working mechanism of NanoSIMS is the same as that of conventional SIMS except for the two unique designs: The coaxial lens and the magnet (detailed in text). NanoSIMS 50L is equipped with two ion sources: Oxygen and cesium, which can produce O^{2-}, O^-, O^+ and Cs^+ primary ion beams, respectively. The diameter of Cs^+ ion beam can be as low as 50 nm. NanoSIMS 50L has 7 detectors, which can simultaneously detect 7 ion species with mass differences of up to 21 times (M_{max}/M_{min}=21).

In order to meet the scientific demands of high spatial resolution, Cameca developed the first NanoSIMS based on the conventional SIMS in 2000. The Cameca NanoSIMS 50L greatly improved the spatial resolution thanks to the coaxial design (Figure 2), which includes a normal primary ion incidence and a co-axial secondary ion extraction to optimize simultaneously objective lens performance and ion collection. This design reduced the objective-sample distance (0.4 mm), leading to very low aberration coefficients and thus to a smaller spot size for a given probe current than other conventional SIMS.

In addition, although both NanoSIMS and conventional SIMS using Mattauch-Herzog double focusing magnet, the magnetic field radius of NanoSIMS has a very wide range of 150–670 mm (Figure 1), whereas that of IMS-1280 is

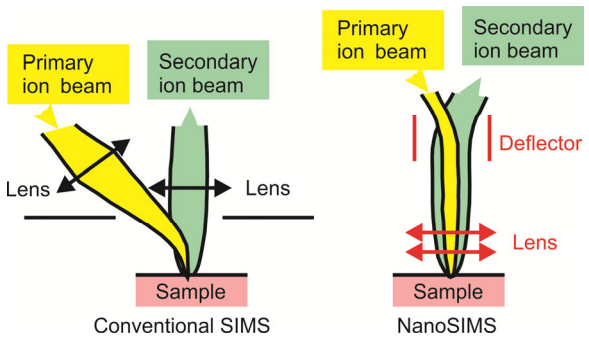

Figure 2 Schematic diagram showing the coaxial design of NanoSIMS 50L.

about 585 mm. Such a wide magnetic field allows NanoSIMS simultaneously detects species with mass differences of up to 21 times (M_{max}/M_{min}=21), e.g., ^{16}O and ^{238}U. However, there is a drawback of this design. Due to the limitation of dispersion distance and the size of detectors (5–6 mm), the mass difference between two adjacent detectors must be larger than $M_{internal}=M_{max}/58$ (Figure 1). For example, when U-Pb dating, NanoSIMS 50L can measure ^{206}Pb and ^{238}U by multi-collection mode, but must use peak-jumping mode to measure ^{206}Pb and ^{207}Pb (Yang et al., 2012).

Same as conventional SIMS, NanoSIMS 50L is equipped with two ion sources: Duoplasmatron oxygen source and thermal ionization cesium source. The former uses oxygen as a plasma source, producing O^{2-}, O^-, O^+ ions, and the latter generates Cs^+ ions by thermal ionization. The size of oxygen ion beam can be as small as 200 nm, whereas that of cesium ion beam can be 50 nm.

1.2 Analytical modes of NanoSIMS

Since NanoSIMS still preserves relatively high mass resolution, sensitivity, and analytical precision, many methods developed by conventional SIMS can also be implemented by NanoSIMS, such as high-precision spot analysis. In addition, other methods which are difficult to be implemented by conventional SIMS, can also be carried out by NanoSIMS due to its high spatial resolution, such as distribution image analysis. There are three analytical modes of NanoSIMS.

(1) The spot analysis is usually applied to the dating or stable isotope analysis (see sections 3 and 4).

(2) The image analysis can obtain an elemental or isotopic distribution image of the sample surface. When a primary ion beam scans on the sample surface, the secondary ions detected by NanoSIMS can reflect elemental and isotopic variation of the scanning area. Therefore elemental or isotopic distribution images can be obtained, based on which the elemental or isotopic variation along any profile can be calculated. This analytical mode has been widely used in space sciences (Hoppe, 2006; Messenger et al., 2003; Zinner et al., 2011) and life sciences (Herrmann et al., 2007; Lechene et al., 2006, 2007; Musat et al., 2008), but rarely applied to earth sciences because the analytical precision of this mode is relatively low.

(3) The grain mode combines image and spot analysis. For example, secondary ion images are first acquired from a relatively large scanning area, and then spot analysis can be carried out in the secondary ion images to conduct a relative high analytical precision (see section 2).

2 Trace element analysis of mineral zonings

Growth zoning is a very common phenomenon of minerals in nature. According to Shore and Fowler (1996), there are at least 75 minerals which can develop oscillatory zonings, including all mineral species, such as silicate (anhydrous or hydrous), sulfide, oxide, halide, carbonate, phosphate, and sulfate. Studies on mineral zonings can reveal the dynamic processes during crystal growth (Carley et al., 2011; Gardner et al., 1995; Hoskin et al., 1998; Klemetti et al., 2011; L'Heureux and Fowler, 1996; Loomis, 1982; Singer et al., 1995; Wang and Merino, 1992) or variations of the geological environments (Gao et al., 2004; Zhang, 2005).

However, the growth zonings of minerals (especially oscillatory zonings) are usually very small (at micron scale). In order to study these zonings, analytical methods with high spatial resolution are required. For example, scanning electron microscope (SEM) and electron probe microanalysis (EPMA) are widely used to reveal the major element variations along the zonings. However, these methods cannot detect trace elements that may provide important information on the mineral growth, because the distributions of trace elements are generally controlled by diffusion and distribution coefficient.

The high spatial resolution and high sensitivity of NanoSIMS make it a potential powerful tool to observe the trace elemental distributions of mineral zonings at micron or sub-micron scales. For example of zircon, Cameca NanoSIMS 50L was used to study trace elemental distributions of the oscillatory zonings. A 100 pA O^- primary ion beam with a diameter of about 0.7 μm was utilized. The whole procedure was divided into two sessions because NanoSIMS 50L can only detect 7 species simultaneously. In the first session, ^{7}Li, ^{29}Si, ^{31}P, ^{49}Ti, ^{89}Y and ^{96}Zr were measured, and then ^{30}Si, ^{89}Y, ^{140}Ce, ^{147}Sm, ^{162}Dy and ^{175}Lu in the second session. Zircon standards 91500 and M257 were used as standards.

The Qinghu magmatic zircons (Li et al., 2013b, 2009) were measured by the grain mode. As shown in Figure 3, a 20 μm× 20 μm area was scanned and secondary ion images were acquired. Then based on the image of ^{89}Y/^{29}Si, eight spot analyses were carried out by deflecting the primary beam onto a selected area (3 μm×3 μm). There is a correlation between zircon Cathodoluminescence (CL) image and

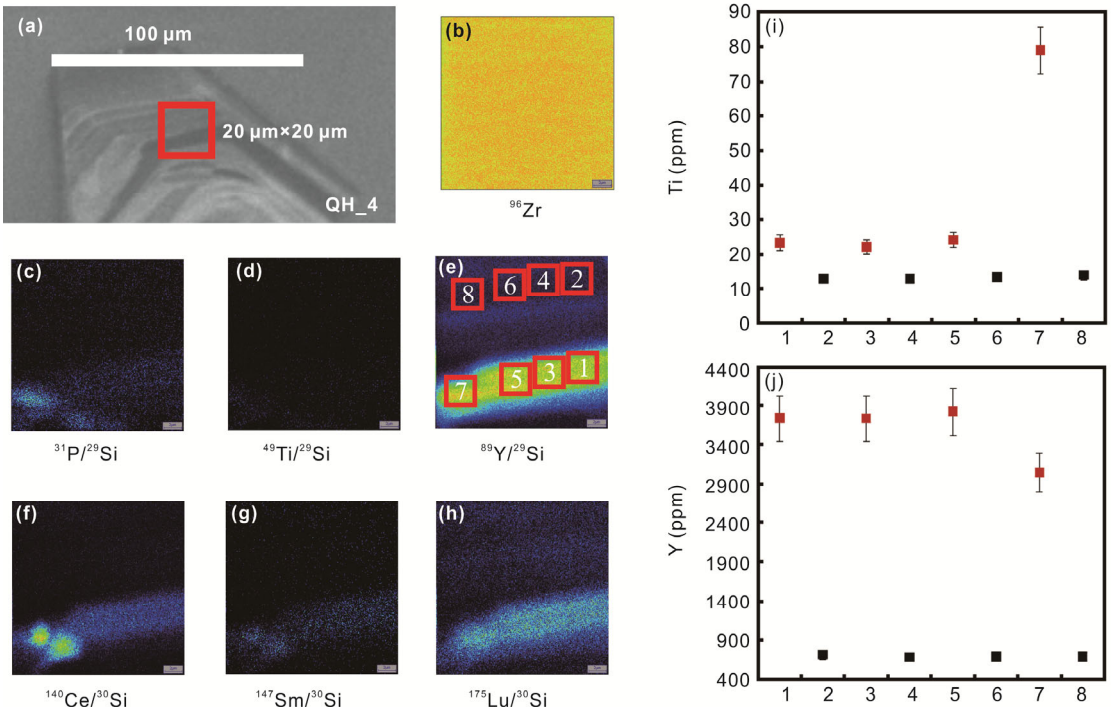

Figure 3 Trace elemental distribution images and Y, Ti spot analysis of zircon QH-4. (a) Cathodoluminescence image of the zircon. (b)–(h) Secondary ion images (using Si as an internal standard). Warm colors (red and yellow) represent relative high count rate, and cold colors (green and blue) represent relative low count rate. (i)–(j) Y and Ti contents of 8 analytical spots, whose positions are shown in (e).

its secondary ion image, with the dark band in CL images having higher P, Y and REE concentration. According to the results of spot analysis, the Y and Ti abundances of the dark bands can be 5–8 times and 1 time higher than those of the bright bands, respectively.

This case study of the Qinghu zircons indicates that the NanoSIMS is capable of analyzing trace elemental distributions in mineral zonings at micron or sub-micron scale. This method can be applied to the fine zonation of all the natural minerals, which has at least three advantages: (1) high spatial resolution, the size of the O^- ion beam is as small as 0.7 μm; (2) low detection limit, trace element of micrograms per gram level can be quantitatively measured; (3) precise positioning, based on the secondary ion images acquired before spot analysis, interference of fractures and micro mineral inclusions can be avoided.

3 High spatial resolution zircon U-Pb/Pb-Pb dating

Zircon is an accessory mineral widely occurring in both terrestrial and extraterrestrial rocks. The high U, Th contents and low common Pb of zircon make it a good U-Pb chronometer. *In situ* zircon U-Pb dating with SIMS is one of the key techniques in the modern earth sciences, and has become a routine method for >20 μm zircons (Ireland and Williams, 2003). However, high spatial resolution is still required because zircons in the lunar meteorites and other extraterrestrial samples are generally very small (<10 μm), and many zircons in terrestrial samples have complex zoning (e.g., zircons in granulites).

Although a zircon U-Pb dating method at 5 μm scale has been established with Cameca IMS-1280 (Liu et al., 2011), NanoSIMS can achieve even higher spatial resolutions for U-Pb and Pb-Pb dating (Yang et al., 2012). A 500 pA O^- primary ion beam with a diameter of 1.7 μm was utilized. Magnetic peak-switching mode was applied for Pb-Pb dating, while combined analysis mode was used for U-Pb dating (Yang et al., 2012).

The zircon standard M257 and baddeleyite standard Phalaborwa were dated by the Pb-Pb method with a spatial resolution of < 2 μm (Figure 4), yielding ^{207}Pb/^{206}Pb ages of 563±14 Ma and 2058±6 Ma, respectively. These results agree well with the recommended ages within analytical uncertainties. Four zircon standards, including Qinghu, Plesovice, Temora, and 91500 were dated by the U-Pb method, with a spatial resolution of < 5 μm (Figure 4). The weighted average ^{206}Pb/^{238}U ages obtained by this method for the four zircon standards are 158±3, 337±7, 427±10, and 1076±14 Ma, respectively. These results are consistent with the reported ID-TIMS ages of these samples within error (Yang et al., 2012).

This method demonstrated that zircon U-Pb dating at <5 μm scale and Pb-Pb dating at <2 μm scale can be achieved with NanoSIMS. However, there is a limitation of this

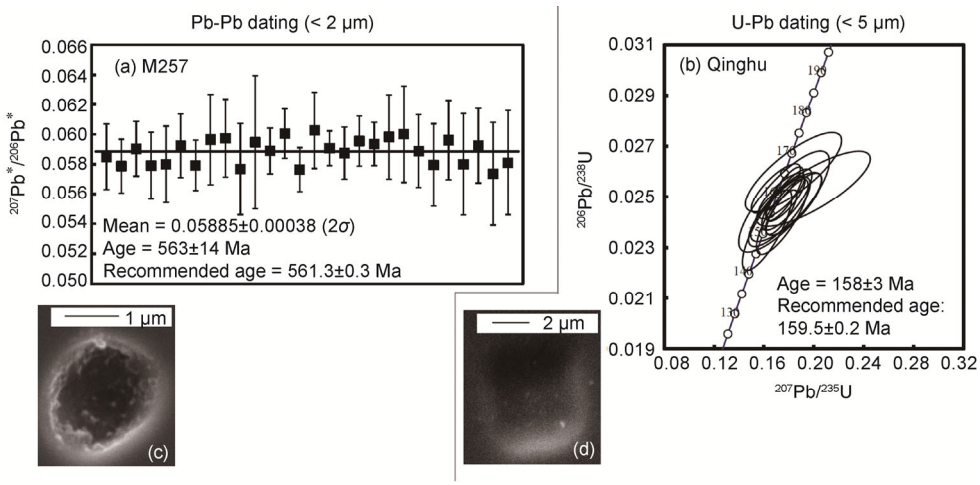

Figure 4 Zircon U-Pb and Pb-Pb dating with high spatial resolutions by NanoSIMS (Yang et al., 2012).

method. When applying it, the sensitivity of Pb is about 4 cps ppm^{-1} nA^{-1}, which is significantly lower than that of IMS-1280 (13–21 cps ppm^{-1} nA^{-1}) by using oxygen flooding technique. Due to this limitation, this method can only be applied to old zircons, such as ~2.0 Ga (Wang et al., 2014).

4 Stable isotope analysis

4.1 Water content and H isotope analysis for silicate glass and apatite

Hydrogen is the lightest element in the universe and has the largest mass-dependent fractionation effects in geological and biological processes, hence can be used to constrain the evolution of climate, geology, and life. In addition, H is the most abundant element in the solar system (Anders and Ebihara, 1982), and is the major constituent element of water, which is usually used as an indicator for searching alien life. Thus, analytical methods *in situ* determining water content and H isotopes are very important for our understanding of the above processes.

There are two common used *in-situ* methods for water content. One is infrared spectra (Aubaud et al., 2007; Koga et al., 2003; Nichols and Wysoczanski, 2007; Prechtel and Stalder, 2010), which has a detection limit lower than 10 ppm. However, this method cannot measure H isotopes. The other method is SIMS, which can determine both water content and H isotopes. However, this method was constrained by the charging effect and high hydrogen background (Deloule et al., 1995; Watson et al., 1994; Zinner et al., 1983). In the recent decade, electron gun (E-gun) was applied to charge compensation and resin-free sample preparation method (see section 6) was used to decrease the hydrogen background. Low background (10–30 ppm) methods have been established with IMS 1270/80 and IMS f series (Greenwood et al., 2008; Hauri et al., 2002; Koga et al., 2003; Sugiura and Hoshino, 2000) with a spatial resolution of 10–30 μm (Bradley et al., 2014; Greenwood et al., 2011, 2014; Hauri et al., 2011; McCubbin et al., 2010).

An analytical method with a higher spatial resolution for water contents and H isotopes has been established by using NanoSIMS 50L. The instrumental configurations are described as follows. A 500 pA Cs^+ primary beam with a diameter of 1μm was used. The scanning area was about 10 μm×10 μm. In order to decrease the H re-deposition effect around the analytical margins, the outmost 50 % areas of the spots were blanked. The total time for each analysis is around 5-8 min. The analysis standards include 2 apatites (Durango and Kovdor apatite) (Greenwood et al., 2008; Nadeau et al., 1999) and 5 basaltic glasses (1833-1, 1833-11, ND 70-01, 519-4-1 and MORB glasses) (Hauri et al., 2002). Anhydrous San Carlos olivine (Aubaud et al., 2007), sapphire, silicon wafer and stainless sample holder were used for monitoring the background.

The results show that the H background is positively correlated with the vacuum of analytical chamber of the NanoSIMS (Hu et al., 2014). When the vacuum reached about 5×10^{-10} tor, the hydrogen background can get down to 10 ppm. Based on 20 months' analysis, Kovdor apatite and MORB glass share a similar hydrogen isotope instrumental mass fractionation within analytical uncertainty, indicating little matrix effect between them. The analytical precisions of hydrogen isotopes for Kovdor apatite (H_2O=0.98 wt.%) and MORB glass (H_2O=0.258 wt.%) are 40 ‰ (2SD) and 61‰ (2SD) (Hu et al., 2014), respectively. The maximum uncertainty of the slopes of the water content calibration curves is lower than 6.9% (2SD).

By using this method, Hu et al. (2014) have measured the water contents and H isotopes of apatites and magmatic inclusions in Martian meteorite GRV 020090. They determined the water contents and H isotopic variations along profiles in magmatic inclusions smaller than 50 μm, and the results indicate that the Mars has underground liquid water

in recent past. This method can also be applied to measure water contents and H isotopes of magmatic inclusions from earth's mantle, which could rebuild the geological processes and water contents of earth's deep interior.

This method has two advantages compared to infrared spectra: (1) *in situ* H isotopes can be determined to reveal distribution of H isotopes in apatites and silicate glasses; (2) the image analyses of NanoSIMS 50L are helpful in identifying the micro-fractures in apatite and silicate glasses, and thus avoid any contamination on water contents and H isotopes.

4.2 Carbon isotope analysis for diamond and graphite

The carbon cycle on the Earth's surface is an important environmental issue, because the balance of which is considered to be the key factor for the climate change. Therefore, global warming and carbon emissions attract considerable attentions. However, the largest carbon reservior of the Earth is the mantle (Coltice et al., 2004). Beside the carbon cycle on the Earth's surface, there is a deep carbon cycle (Zhang and Zindler, 1993). The flux of deep carbon cycle is significantly larger than that on the surface, becoming a buffer for the surface carbon cycle. Diamond is an important carrier of the mantle carbon; thus, its formation and evolution can help us understand the deep carbon cycle (Pokhilenko et al., 2004; Russell et al., 1996). The C and N isotopic compositions of diamonds could record the information of their source, and the growth zonings in diamonds could reflect the processes during their formation (Boyd et al., 1987; Dobrzhinetskaya et al., 2007; Eldridge et al., 1991).

Carbon isotope measurements were usually carried out by SIMS with a precision of ~0.1‰ and a spatial resolution of 15–30 μm (Farquhar et al., 1999; Fitzsimons et al., 1999; Palot et al., 2014; Riciputi et al., 1998; Russell et al., 1996; Smart et al., 2011). However, zonings are very common in diamonds, which may reflect complex processes during their growth, and the spatial resolution of the above methods is insufficient to reveal these processes.

To improve the spatial resolution of the carbon isotopic measurement in graphite and diamond, two instrumental configurations were carried out for different requirements (3–10 μm).

(1) FC-EM mode: ^{12}C and ^{13}C were measured with the FC and the EM, respectively. A 100 pA Cs^+ primary beam with a diameter of 0.5 μm was used to raster over an area of 3 μm× 3 μm. The precision of $\delta^{13}C$ on the graphite standard was ~0.4‰ (Figure 5).

(2) FC-FC mode: Both of ^{12}C and ^{13}C were measured with the FCs. A 800 pA Cs^+ primary beam with a diameter of 1 μm was used to rater over an area of 10 μm×10 μm. The precision of $\delta^{13}C$ on the graphite standard was ~0.3‰ (Figure 5).

These two instrumental configurations were performed with grain mode. Secondary ion images of ^{12}C and $^{12}C^{14}N$ were obtained to identify zonings with variable N contents. Then, regions of interest were selected to carbon isotopic analysis. The sizes of analytical spots were 3 and 10 μm for FC-EM and FC-FC mode, respectively. Both graphite and diamond were measured by this method. The results show that the matrix effect between graphite and diamond was as little as ~0.7‰ (Figure 5).

In summary, carbon isotope measurements at 3–10 μm scale can be achieved with NanoSIMS. For 5–10 μm spatial resolution, a precision of ~0.3‰ can be obtained by FC-FC mode. For 3–5 μm, a precision of ~0.4‰ can be obtained by FC-EM mode. Compared to the methods established by conventional SIMS, which have lateral resolutions of 15–30 μm and precisions of ~0.1‰, this method improves spatial resolution significantly but has relatively low precision. Therefore, this method can meet high spatial resolution requirements, e.g., diamond with complex zonings, micro particles of graphite, diamond and organic carbon in the meteorites.

4.3 Oxygen isotope analysis for carbonate

The oxygen isotopes of carbonates have been widely used as a tracer for paleo-environment and paleoclimate evolutions. The oxygen isotopes of marine carbonate fossils can help us reconstruct the temperature variations of the ocean

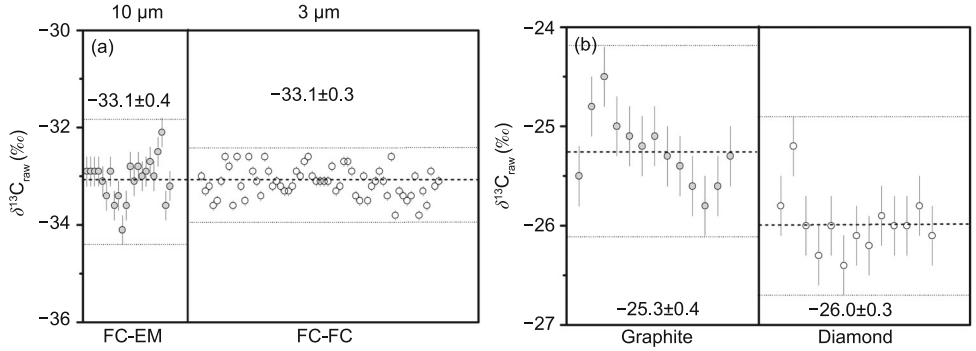

Figure 5 Carbon isotope analysis of diamond and graphite by NanoSIMS. The spatial resolution and precision were 3 μm and 0.4‰ for FC-EM mode, and 10μm and 0.3‰ for FC-EM mode. The matrix effect between graphite and diamond was insignificant (~0.7‰).

since Cenozoic (Craig, 1965). For example, $\delta^{18}O$ values of speleothem can reflect those of rain and water during its formation, and *in situ* oxygen isotopic analysis provides a powerful method to reveal the paleoclimate evolutions (Affek et al., 2008). However, this brings challenges in analytical technique. The growth zoning in speleothem is always narrow, requiring a high spatial resolution. In addition, the oxygen isotope variations in the zonings are generally small, requiring a high precision (Orland et al., 2012).

For example, the spatial resolutions of carbonate oxygen isotopic analysis by using SIMS are ~10 μm and the analytical precision is 0.3‰ (2SD) (Kita et al., 2009; Orland et al., 2012). These method were widely used to measure the oxygen isotopic variation in samples with growth zonings (e.g., cave speleothem) (Orland et al., 2012). However, such a spatial resolution is still insufficient for the measurement of the growth zonings at several microns scale.

High spatial resolution analysis of oxygen isotopes can be carried out by NanoSIMS 50L. A ~250 pA primary Cs+ beam with a diameter of ~0.5 μm was used to scan 5 μm× 5μm area on the sample. $^{16}O^-$ is counted with a Faraday cup (FC), and $^{18}O^-$ with an electron multiplier (EM). Two reference materials of calcite NBS 18 ($\delta^{18}O_{VPDB}$=(−23.2± 0.1)‰) and IAEA-CO-8 ($\delta^{18}O_{VPDB}$=(−22.7±0.2)‰) were used as standards (Stichler, 1995). The results are plotted in Figure 6. The analytical precision is better than 0.5‰ (1 SD).

Same as carbon isotope analysis, oxygen isotope analysis of NanoSIMS also has a high spatial resolution (5 μm) with a relatively low precision. Therefore, this method can be applied to the abrupt interface in speleothem, where oxygen isotopic variation is large and high spatial resolution is required. In addition, the multi-collection capability of NanoSIMS allows detection of other trace element (e.g., Sr) simultaneously.

4.4 Sulfur isotope analysis for sulfides

Sulfides are common minerals occurred in sedimentary rocks, volcanic rocks, and meteorites, which include pyrite, pyrrhotite, chalcopyrite, sphalerite, galena, etc. The S isotopic compositions of these minerals are widely used to study atmospheric activities (Winterholler et al., 2006), microbial activities (Bontognali et al., 2012; Nishizawa et al., 2010), ore-forming mechanism (Barker et al., 2009), and the early evolution of the Earth's surface environment (Mojzsis et al., 2003).

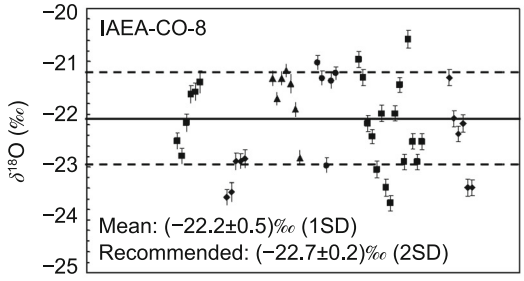

Figure 6 The results of oxygen isotope analysis on IAEA-CO-8 calcite standards (Lin et al., 2014). The result was calibrated using NBS 18 as a standard. The measured $\delta^{18}O_{VPDB}$ (−22.2±0.2)‰ is consistent with the recommended value within the analytical uncertainties.

In situ analysis of S isotopes is generally performed using SIMS or laser ablation inductively coupled plasma mass spectrometry (LA-ICPMS). LA-ICP-MS has little matrix effect for S isotope analysis of sulfides, but has a poor lateral resolution (50–100 μm) (Craddock et al., 2008). In addition, ^{36}S cannot be precisely measured by LA-ICP-MS, because it is suffered from severe interference of ^{36}Ar. Compared to LA-ICPMS, SIMS has a better lateral resolution (~15 μm) and precision (0.1‰–0.2‰) (Kozdon et al., 2010; Mojzsis et al., 2003; Papineau et al., 2005; Whitehouse, 2013). However, this lateral resolution of SIMS is still insufficient to analyze the micron-sized sulfide with the biogenic origin (e.g., framboidal pyrite) and the narrow zonings in the sulfide formed by the hydrothermal and metamorphic processes.

High spatial resolution of <1 μm can be achieved by S isotopic measurements with NanoSIMS 50L (Zhang et al., 2014). The international standard pyrites of Balmat and CAR123 and working reference of 1117 were used as standards. To meet the requirements of different lateral resolutions, three instrumental configurations were carried out.

(1) FC-FC-FC-EM mode: High analytical precision was achieved by counting ^{32}S, ^{33}S and ^{34}S with the FCs and ^{36}S with the EM. A 400 pA Cs^+ primary beam with a diameter of 1 μm was used to scan over areas of 5 μm×5 μm. The standard deviations of spot-to-spot and grain-to-grain (external reproducibility 1 SD) measurements were better than 0.3‰, 0.3‰ and 0.7‰ for $\delta^{33}S$, $\delta^{34}S$ and $\delta^{36}S$, respectively (Figure 7).

(2) FC-EM-EM-EM mode: ^{32}S was measured with the FC and the other signals were measured with the EMs. A 7 pA Cs^+ primary beam with a diameter of 0.3 μm was used to scan over areas of 2 μm×2 μm. The external reproducibility (1SD) was better than 0.5‰ for both $\delta^{33}S$ and $\delta^{34}S$ and was 1.5‰ for $\delta^{36}S$ (Figure 7).

(3) EM-EM-EM mode: ^{32}S, ^{33}S and ^{34}S were measured with EMs. A 0.7 pA Cs^+ primary beam with a diameter of 0.1 μm was used to scan over areas of 1 μm×1 μm. The external reproducibility (1 SD) was better than 1‰ for both $\delta^{33}S$ and $\delta^{34}S$ (Figure 7).

Sulfur isotope analysis with NanoSIMS 50L has the following advantages: (1) it has a high spatial resolution, e.g., EM-EM-EM mode < 1 μm, which is the only method capable of measuring S isotopic composition at a sub-micron scale, e.g., framboidal pyrite; (2) ^{36}S could be measured by FC-FC-FC-EM and FC-EM-EM-EM modes; (3) trace element distribution can be obtained by grain mode simultaneously, e.g., As and Au.

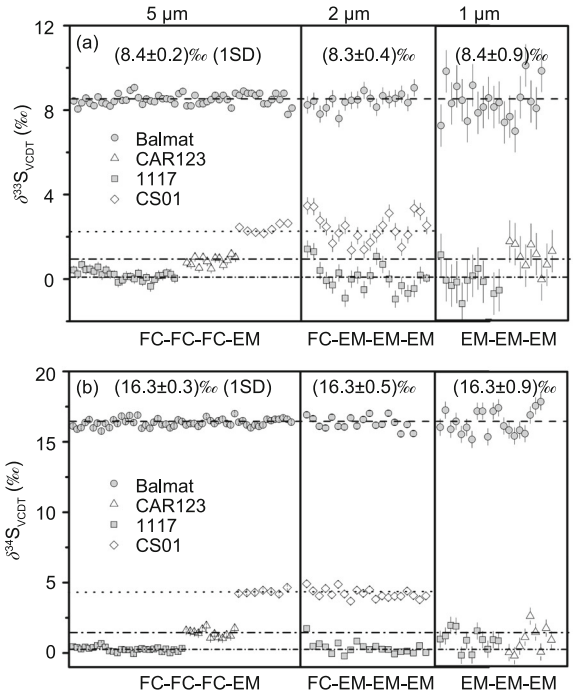

Figure 7 The result of sulfur isotopes of standard sulfides measured with NanoSIMS. For three modes, spatial resolution and the precision were 5 μm, 2 μm, 1 μm and 0.3‰, 0.5‰, 1‰ for $\delta^{33}S$ and $\delta^{34}S$, respectively. The samples are international standard pyrites Balmat and CAR123, and working reference of 1117 pyrite.

5 Sample preparation

There are three basic requirements for the sample preparation of SIMS.

(1) Non-volatile solid samples. In order to keep a high vacuum of the analysis chamber, NanoSIMS cannot analyze liquid and volatile samples.

(2) A smooth sample surface. Previous study revealed that both the precision and accuracy of the SIMS were affected by the smoothness of the sample surface (Kita et al., 2009). Therefore, to obtain accurate results, polishing is required to make the sample surface as smooth as possible.

(3) A conductive sample. For non-conductive samples (e.g., rocks), coating with gold or carbon is required before analysis.

Beside the above three basic requirements, there are two more for NanoSIMS analysis.

(1) Size of sample mount. The sample mount must be prepared to be round with a diameter of 25.4 mm, 12.7 mm or 10 mm (Figure 8).

(2) Volatility of sample mount. Minerals or rocks are generally embedded in resin to prepare a round sample mount for SIMS analysis. However, when using this method to prepare sample for NanoSIMS analysis, particular attention should be paid to the selection of resin, because the requirement of vacuum level of the NanoSIMS analysis chamber is higher than that of conventional SIMS. Therefore, resins with little degassing effect under high vacuum conditions should be selected. In addition, the usage amount of resin should be as little as possible (e.g., cut or grind sample mount to 100–300 μm thick, and then put it up on a round sheet glass with same diameter).

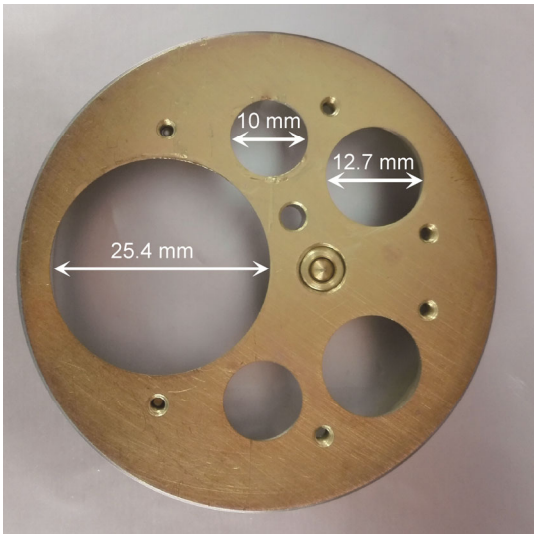

Figure 8 A type of sample holder for NanoSIMS analysis, which can load five sample mounts or thin sections with variable diameters.

For different samples, three sample preparation methods are recommended.

(1) Microbial or micro-particle samples (e.g., $PM_{2.5}$) can be dropped with water on a round shape silicate wafer or gold leaf. After dried in an oven, the sample is ready for analysis, because both silicate wafer and gold leaf are conductive.

(2) Rock, mineral or material samples can be embedded into a resin mount. After grinded and polished, the sample mount should be coated with gold or carbon before put into the instrument. When using this method, particular attention should be paid to the selection of resin. Resins with little degassing effect under high vacuum conditions are required.

(3) For water content and H isotope analysis, since the vacuum of analysis chamber significantly affects the analytical background, sample mount cannot be made of any kind of resin. Specific sample preparation steps are as follows: First, soluble resin (such as crystalbond, a kind of purified rosin) was used to embed samples. After grinded and polished, the sample mount was then washed 5–6 times (interval 4–6 hours each) by acetone to ensure that the resin was completely removed. Finally, the sample was dried at 105 °C for 12 hours, and then pressed into a metal indium mount. Coating with gold or carbon is also required if the sample is non-conductive.

6 Summary

The first NanoSIMS of China (Cameca NanoSIMS 50L)

was installed at Institute of Geology and Geophysics, Chinese Academy of Sciences in 2011. This instrument has 7 detectors, and can detect 7 species with up to 21 times mass difference (M_{max}/M_{min}=21) simultaneously. The NanoSIMS has two ion sources, Cs and O. The minimum size of O^- ion beam can reach 200 nm, and that of Cs^+ can be as small as 50 nm. The NanoSIMS can carry out both high precision spot analysis and high spatial resolution image analysis.

In order to meet the analytical requirements of earth sciences, we have established a variety of analytical methods with the NanoSIMS, which include trace element distribution images in mineral zoning, high spatial resolution (2–5 μm) Pb-Pb and U-Pb dating, water content and H isotopic analysis for silicate glass and apatite, C isotopic analysis for diamond and graphite, O isotopic analysis for carbonate, S isotopic analysis for sulfides.

We thank the reviewers for their constructive suggestions and commons. This work was supported by the National Natural Science Foundation of China (Grants Nos. 41173012, 41103031, 41230209, 41322022, 41221002).

Affek H P, Bar-Matthews M, Ayalon A, et al. 2008. Glacial/interglacial temperature variations in Soreq cave speleothems as recorded by "clumped isotope" thermometry. Geochim Cosmochim Acta, 72: 5351–5360

Anders E, Ebihara M. 1982. Solar-system abundances of the elements. Geochim Cosmochim Acta, 46: 2363–2380

Aubaud C, Withers A C, Hirschmann M M, et al. 2007. Intercalibration of FTIR and SIMS for hydrogen measurements in glasses and nominally anhydrous minerals. Am Mineral , 92: 811–828

Badro J, Ryerson F J, Weber P K, et al. 2007. Chemical imaging with NanoSIMS: A window into deep-Earth geochemistry. Earth Planet Sci Lett, 262: 543–551

Barker S L L, Hickey K A, Cline J S, et al. 2009. Uncloaking invisible gold: use of NanoSIMS to evaluate gold, trace elements, and sulfur isotopes in pyrite from Carlin-type gold deposites. Econ Geol, 104: 897–904

Bontognali T R R, Sessions A L, Allwood A C, et al. 2012. Sulfur isotopes of organic matter preserved in 3.45-billion-year-old stromatolites reveal microbial metabolism. Proc Natl Acad Sci USA, 109: 15146–15151

Boyd S R, Mattey D P, Pillinger C T, et al. 1987. Multiple growth events during diamond genesis: An integrated study of carbon and nitrogen isotopes and nitrogen aggregation state in coated stones. Earth Planet Sci Lett , 86: 341–353

Bradley J P, Ishii H A, Gillis-Davis J J, et al. 2014. Detection of solar wind-produced water in irradiated rims on silicate minerals. Proc Natl Acad Sci USA, 111: 1732–1735

Carley T, Miller C, Wooden J, et al. 2011. Zircon from historic eruptions in Iceland: Reconstructing storage and evolution of silicic magmas. Mineral Petrol, 102: 135–161

Coltice N, Simon L, Lecuyer C. 2004. Carbon isotope cycle and mantle structure. Geophys Res Lett, 31: L05603

Craddock P R, Rouxel O J, Ball L A, et al. 2008. Sulfur isotope measurement of sulfate and sulfide by high-resolution MC-ICP-MS. Chem Geol, 253: 102–113

Craig H. 1965. The measurement of oxygen isotope paleotemperatures. In: Tongiorgi E, ed. Stable Isotopes in Oceanographic Studies and Paleotemperatures. Spoleto: Lab Geol Nucl Pisa. 161–182

Dark C, Kilburn M R, Hammerl G, et al. 2006. NanoSIMS analysis of Ca doping at a grain boundary in a superconducting YBCO Ca-123/123 bicrystal. J Phys-Conf Ser, 43: 272–276

Deloule E, Paillat O, Pichavant M, et al. 1995. Ion microprobe determination of water in Silicate-Glasses: Methods and applications. Chem Geol, 125: 19–28

Dobrzhinetskaya L F, Wirth R, Green H W. 2007. A look inside of diamond-forming media in deep subduction zones. Proc Natl Acad Sci USA, 104: 9128–9132

Eldridge C S, Compston W, Williams I S, et al. 1991. Isotope evidence for the involvement of recycled sediments in diamond formation. Nature, 353: 649–653

Farquhar J, Hauri E, Wang J. 1999. New insights into carbon fluid chemistry and graphite precipitation: SIMS analysis of granulite facies graphite from Ponmudi, South India. Earth Planet Sci Lett, 171: 607–621

Fitzsimons I, Harte B, Chinn I, et al. 1999. Extreme chemical variation in complex diamonds from George Creek, Colorado: A SIMS study of carbon isotope composition and nitrogen abundance. Mineral Mag, 63: 857–857

Gao S, Rudnick R L, Yuan H L, et al. 2004. Recycling lower continental crust in the North China craton. Nature, 432: 892–897

Gardner J, Carey S, Rutherford M, et al. 1995. Petrologic diversity in Mount St. Helens dacites during the last 4000 years: Implications for magma mixing. Contrib Mineral Petrol , 119: 224–238

Greenwood J, Itoh S, Sakamoto N, et al. 2014. Hydrogen isotopes of water in the moon: Evidence for the giant impact model from melt inclusions and apatite in apollo rock samples. Lunar and Planetary Institute Science Conference Abstracts. 2707

Greenwood J, Itoh S, Sakamoto N, et al. 2008. Hydrogen isotope evidence for loss of water from Mars through time. Geophys Res Lett, 35: L05203

Greenwood J, Itoh S, Sakamoto N. et al. 2011. Hydrogen isotope ratios in lunar rocks indicate delivery of cometary water to the Moon. Nature, 4: 1–4

Hauri E, Wang J, Dixon J E, et al. 2002. SIMS analysis of volatiles in silicate glasses: 1. Calibration, matrix effects and comparisons with FTIR. Chem Geol, 183: 99–114

Hauri E, Weinreich T, Saal A E, et al. 2011. High pre-eruptive water contents preserved in lunar melt inclusions. Science, 333: 213–215

Herrmann A M, Ritz K, Nunan N, et al. 2007. Nano-scale secondary ion mass spectrometry—A new analytical tool in biogeochemistry and soil ecology: A review article. Soil Biol Biochem, 39: 1835–1850

Hoppe P. 2006. NanoSIMS: A new tool in cosmochemistry. Appl Surf Sci, 252: 7102–7106

Hoskin P, Arslan M, Aslan Z, et al. 1998. Clinopyroxene phenocryst formation in an alkaline magma: Interpretations from oscillatory zoning. Mineral Mag, 62: 653–654

Hsu W B. 2005. Ion Microprobe Techniques and Applications in Cosmochemistry and Geochemistry. Geological Journal of China Universities, 11: 239-252

Hu S, Lin Y, Zhang J, et al. 2014. NanoSIMS analyses of apatite and melt inclusions in the GRV 020090 Martian meteorite: Hydrogen isotope evidence for recent past underground hydrothermal activity on Mars. Geochim Cosmochim Acta, 140: 321–333

Ireland T R, Williams I S. 2003. Considerations in Zircon Geochronology by SIMS. Rev Mineral Geochem, 53: 215–241

Kita N T, Ushikubo T, Fu B, et al. 2009. High precision SIMS oxygen isotope analysis and the effect of sample topography. Chem Geol, 264: 43–57

Klemetti E W, Deering C D, Cooper K M, et al. 2011. Magmatic perturbations in the Okataina Volcanic Complex, New Zealand at thousand-year timescales recorded in single zircon crystals. Earth Planet Sci Lett, 305: 185–194

Koga K, Hauri E, Hirschmann M, et al. 2003. Hydrogen concentration analyses using SIMS and FTIR: Comparison and calibration for nominally anhydrous minerals. Geochem Geophys Geosyst, 4: 1019, doi: 10.1029/2002GC000378

Kozdon R, Kita N T, Huberty J M, et al. 2010. In situ sulfur isotope analysis of sulfide minerals by SIMS: Precision and accuracy, with application to thermometry of 3.5Ga Pilbara cherts. Chem Geol, 275: 243–253

L'Heureux I, Fowler A D. 1996. Dynamical model of oscillatory zoning in plagioclase with nonlinear partition relation. Geophys Res Lett, 23: 17–20

Lechene C, Hillion F, McMahon G, et al. 2006. High-resolution quantita-

tive imaging of mammalian and bacterial cells using stable isotope mass spectrometry. J Biol, 5: 20
Lechene C P, Luyten Y, McMahon G, et al. 2007. Quantitative Imaging of Nitrogen Fixation by Individual Bacteria Within Animal Cells. Science, 317: 1563–1566
Li X, Tang G, Gong B, et al. 2013. Qinghu zircon: A working reference for microbeam analysis of U-Pb age and Hf and O isotopes. Chin Sci Bull, 58: 4647–4654
Li X, Liu Y, Li Q L, et al. 2009. Precise determination of Phanerozoic zircon Pb/Pb age by multicollector SIMS without external standardization. Geochem Geophys Geosyst, 10: Q04010, doi: 10.1029/2009GC002400
Lin Y, Feng L, Hao J, et al. 2014. Sintering nano-crystalline calcite: A new method of synthesizing homogeneous reference materials for SIMS analysis. J Anal At Spectrom, 29:1686–1691
Liu Y, Li X H, Li Q L, et al. 2011. Precise U-Pb zircon dating at a scale of <5 micron by the CAMECA 1280 SIMS using a Gaussian illumination probe. J Anal At Spectrom, 26: 845–851
Loomis T. 1982. Numerical simulations of crystallization processes of plagioclase in complex melts: The origin of major and oscillatory zoning in plagioclase. Contrib Mineral Petrol , 81: 219–229
McCubbin F M, Steele A, Hauri E H, et al. 2010. Nominally hydrous magmatism on the Moon. Proc Natl Acad Sci USA, 107: 11223–11228
McPhail D. 2006. Applications of Secondary Ion Mass Spectrometry (SIMS) in materials science. J Mater Sci, 41: 873–903
Meibom A, Cuif J P, Houlbreque F, et al. 2008. Compositional variations at ultra-structure length scales in coral skeleton. Geochim Cosmochim Acta, 72: 1555–1569
Messenger S, Keller L P, Stadermann F J, et al. 2003. Samples of stars beyond the solar system: Silicate grains in interplanetary dust. Science, 300: 105–108
Mojzsis SJ, Coath C D, Greenwood J P, et al. 2003. Mass-independent isotope effects in Archean (2.5 to 3.8 Ga) sedimentary sulfides determined by ion microprobe analysis. Geochim Cosmochim Acta, 67: 1635–1658
Musat N, Halm H, Winterholler B, et al. 2008. A single-cell view on the ecophysiology of anaerobic phototrophic bacteria. Proc Natl Acad Sci USA, 105: 17861–17866
Nadeau S L, Epstein S, Stolper E. 1999. Hydrogen and carbon abundances and isotopic ratios in apatite from alkaline intrusive complexes, with a focus on carbonatites. Geochim Cosmochim Acta, 63: 1837–1851
Nichols A, Wysoczanski R. 2007. Using micro-FTIR spectroscopy to measure volatile contents in small and unexposed inclusions hosted in olivine crystals. Chem Geol, 242: 371–384
Nishizawa M, Maruyama S, Urabe T, et al. 2010. Micro-scale (1.5 μm) sulphur isotope analysis of contemporary and early archean pyrite. Rapid Commun Mass Sp, 24: 1397–1404
Orland I J, Bar-Matthews M, Ayalon A, et al. 2012. Seasonal resolution of Eastern Mediterranean climate change since 34 ka from a Soreq Cave speleothem. Geochim Cosmochim Acta, 89: 240–255
Page F Z, Ushikubo T, Kita N T, et al. 2007. High-precision oxygen isotope analysis of picogram samples reveals 2 μm gradients and slow diffusion in zircon. Am Mineral, 92: 1772–1775
Palot M, Pearson D, Stern R, et al. 2014. Isotopic constraints on the nature and circulation of deep mantle C–H–O–N fluids: Carbon and nitrogen systematics within ultra-deep diamonds from Kankan (Guinea). Geochim Cosmochim Acta, 139: 26–46
Papineau D, Mojzsis S J, Coath C D, et al. 2005. Multiple sulfur isotopes of sulfides from sediments in the aftermath of Paleoproterozoic glaciations. Geochim Cosmochim Acta, 69: 5033–5060
Pokhilenko N P, Sobolev N V, Reutsky V N, et al. 2004. Crystalline inclusions and C isotope ratios in diamonds from the Snap Lake/King Lake kimberlite dyke system: Evidence of ultradeep and enriched lithospheric mantle. Lithos, 77: 57–67
Prechtel F, Stalder R. 2010. FTIR spectroscopy with a focal plane array detector: A novel tool to monitor the spatial OH-defect distribution in single crystals applied to synthetic enstatite. Am Mineral, 95: 888–891
Riciputi L R, Paterson B A, Ripperdan R L. 1998. Measurement of light stable isotope ratios by SIMS: Matrix effects for oxygen, carbon, and sulfur isotopes in minerals 33 Dedicated to the memory of Al Nier. Int J Mass Spectrom, 178: 81–112
Russell S S, Arden J W, Pillinger C T. 1996. A carbon and nitrogen isotope study of diamond from primitive chondrites. Meteorit Planet Sci, 31: 343–355
Shore M, Fowler A D. 1996. Oscillatory zoning in minerals: A common phenomenon. Can Mineral, 34: 1111–1126
Singer B S, Dungan M A, Layne G D. 1995. Textures and Sr, Ba, Mg, Fe, K, and Ti compositional profiles in volcanic plagioclase: clues to the dynamics of calc-alkaline magma chambers. Am Mineral, 80: 776–798
Smart K A, Chacko T, Stachel T, et al. 2011. Diamond growth from oxidized carbon sources beneath the Northern Slave Craton, Canada: A δ^{13}C–N study of eclogite-hosted diamonds from the Jericho kimberlite. Geochim Cosmochim Acta, 75: 6027–6047
Stichler W. 1995. Interlaboratory comparison of new materials for carbon and oxygen isotope ratio measurements. Reference and Intercomparison Materials for Stable Isotopes of Light Elements, IAEA-TECDOC-825: 67–74
Sugiura N, Hoshino H. 2000. Hydrogen-isotopic compositions in Allan Hills 84001 and the evolution of the martian atmosphere. Meteorit Planet Sci, 35: 373–380
Wang W, Liu X, Hu J, et al. 2014. Late Paleoproterozoic medium-P high grade metamorphism of basement rocks beneath the northern margin of the Ordos Basin, NW China: Petrology, phase equilibrium modelling and U-Pb geochronology. Precambrian Res, 251: 181–196
Wang Y, Merino E. 1992. Dynamic model of oscillatory zoning of trace elements in calcite: Double layer, inhibition, and self-organization. Geochim Cosmochim Acta, 56: 587–596
Watson L L, Hutcheon I D, Epstein S, et al. 1994. Water on Mars: Clues from deuterium/hydrogen and water contents of hydrous phases in SNC meteorites. Science, 265: 86–90
Whitehouse M J. 2013. Multiple sulfur isotope determination by SIMS: Evaluation of reference sulfides for Δ^{33}S with observations and a case study on the determination of Δ^{36}S. Geostand Geoanal Res, 37: 19–33
Winterholler B, Hoppe P, Andreae M O, et al. 2006. Measurement of sulfur isotope ratios in micrometer-sized samples by NanoSIMS. Appl Surf Sci, 252: 7128–7131
Yang W, Lin Y T, Zhang J C, et al. 2012. Precise micrometre-sized Pb-Pb and U-Pb dating with NanoSIMS. J Anal At Spectrom, 27: 479–487
Zhang H F. 2005. Transformation of lithospheric mantle through peridotite-melt reaction: A case of Sino-Korean craton. Earth Planet Sci Lett , 237: 768–780
Zhang J, Lin Y, Yang W, et al. 2014. Improved precision and spatial resolution of sulfur isotope analysis using NanoSIMS. J Anal At Spectrom, 29: 1934–1943
Zhang Y, Zindler A. 1993. Distribution and evolution of carbon and nitrogen in Earth. Earth Planet Sci Lett , 117: 331–345
Zinner E, McKeegan K D, Walker R M. 1983. Laboratory measurements of D/H ratios in interplanetary dust. Nature, 305: 119–121
Zinner E K, Moynier F, Stroud R M. 2011. Laboratory technology and cosmochemistry. Proc Natl Acad Sci USA, 108: 19135–19141